Angstrom-Resolved Interfacial Structure in Buried Organic-Inorganic Junctions

Craig P. Schwartz,[1,*] Sumana L. Raj,[2] Sasawat Jamnuch,[3] Chris J. Hull,[1,2] Paolo Miotti,[4,5] Royce K. Lam,[1,2] Dennis Nordlund,[6] Can B. Uzundal,[2] Chaitanya Das Pemmaraju,[7] Riccardo Mincigrucci,[8] Laura Foglia,[8] Alberto Simoncig,[8] Marcello Coreno,[9,10] Claudio Masciovecchio,[8] Luca Giannessi,[8,10] Luca Poletto,[4] Emiliano Principi,[8] Michael Zuerch,[2,11,12,13] Tod A. Pascal,[3,14,15] Walter S. Drisdell,[1,16,†] and Richard J. Saykally[1,2,‡]

[1]*Chemical Sciences Division, Lawrence Berkeley National Laboratory, Berkeley, California 94720, USA*
[2]*Department of Chemistry, University of California, Berkeley, California 94720, USA*
[3]*ATLAS Materials Science Laboratory, Department of NanoEngineering and Chemical Engineering, University of California, San Diego, La Jolla, California 92023, USA*
[4]*Institute of Photonics and Nanotechnologies, National Research Council of Italy, via Trasea 7, I-35131 Padova, Italy*
[5]*Department of Information Engineering, University of Padova, via Gradenigo 6/B, I-35131 Padova, Italy*
[6]*Stanford Synchrotron Radiation Lightsource, SLAC National Accelerator Laboratory, Menlo Park, California 94025, USA*
[7]*Stanford Institute for Materials and Energy Sciences, SLAC National Accelerator Laboratory, Menlo Park, California 94025, USA*
[8]*Elettra-Sincrotrone Trieste S.C.p.A., Strada Statale 14—km 163.5, 34149 Trieste, Italy*
[9]*ISM-CNR, Istituto di Struttura della Materia, LD2 Unit, 34149 Trieste, Italy*
[10]*Istituto Nazionale di Fisica Nucleare, Laboratori Nazionali di Frascati, Via E. Fermi 54, 00044 Frascati, Italy*
[11]*Materials Sciences Division, Lawrence Berkeley National Laboratory, Berkeley, California 94720, USA*
[12]*Institute for Optics and Quantum Electronics, Abbe Center of Photonics, University of Jena, 07745 Jena, Germany*
[13]*Fritz Haber Institute of the Max Planck Society, 14195 Berlin, Germany*
[14]*Materials Science and Engineering, University of California San Diego, La Jolla, California 92023, USA*
[15]*Sustainable Power and Energy Center, University of California San Diego, La Jolla, California 92023, USA*
[16]*Joint Center for Artificial Photosynthesis, Lawrence Berkeley National Laboratory, Berkeley, California 94720, USA*

(Received 24 February 2021; accepted 2 July 2021; published 24 August 2021)

Charge transport processes at interfaces play a crucial role in many processes. Here, the first soft x-ray second harmonic generation (SXR SHG) interfacial spectrum of a buried interface (boron–Parylene N) is reported. SXR SHG shows distinct spectral features that are not observed in x-ray absorption spectra, demonstrating its extraordinary interfacial sensitivity. Comparison to electronic structure calculations indicates a boron-organic separation distance of 1.9 Å, with changes of less than 1 Å resulting in easily detectable SXR SHG spectral shifts (ca. hundreds of milli-electron volts).

DOI: 10.1103/PhysRevLett.127.096801

Surfaces and interfaces play central roles in a variety of critical biological systems, electronics, batteries, and catalytic systems. Key chemical reactions and physical processes depend explicitly on the electronic structure of the interface and the dynamics across it. Experimentally, surfaces are often studied using a range of spectroscopic and imaging techniques, from grazing incidence x-ray scattering [1,2], to scanning probe [3,4] and total internal reflection [5–7] spectroscopies. These methods, however, are unsuited for the study of *buried* functional interfaces, which often govern critical chemical and physical processes. Interfaces between two bulk materials, or surfaces coated with macroscopically thick (hundreds of nanometers or greater) capping layers, cannot be specifically probed using these techniques. Absorption of photons by the bulk materials prevents optical probes from even reaching such interfaces, and the photoelectrons generated at the buried interface by high penetration x-ray probes cannot escape. Visible and IR second harmonic generation (SHG) and sum frequency generation (SFG) [8,9] do not suffer from these limitations of studying buried interfaces. These techniques have been used for a variety of applications including characterization of semiconductors, solar cell devices, and biological structures [10–12]. While these techniques are quite powerful, they typically provide information about vibrational dynamics or valence transitions, and lack the elemental specificity of x-ray techniques.

Until recently, x-ray nonlinear spectroscopy was precluded by the lack of available light sources with sufficient coherence and flux, but the recent advent of x-ray free electron lasers (FELs) that generate femtosecond pulses with high peak powers and coherence has enabled such experiments [13–15]. Soft x-ray SHG (SXR SHG) offers powerful advantages compared to other surface-specific techniques [16,17]: it has high penetration depth and combines the element specificity of x-ray absorption spectroscopy with the interfacial specificity of second order nonlinear spectroscopies. Linear x-ray absorption

spectroscopy (XAS) is a general tool for studying compounds as it is element specific and sensitive to the chemical and molecular environment of a target atom. Element-specific measurements of core-to-valence transitions can resolve individual contributions to the electronic structure, which is not easily possible in optical spectroscopies that detect valence-to-valence or vibrational transitions. This is especially important for disentangling the contributions from hybridization at interfaces.

While x rays are highly penetrating, the use of different detection methods provides a range of depth sensitivities: transmission measurements are bulk sensitive, fluorescence detection is sensitive to approximately 1 μm thick slabs based on the penetration of the photons [18], and photoelectron or total electron yield (TEY) detection provides sensitivity of a few nanometers due to the limited escape depth of photoelectrons [19–23]. Exploiting soft x-ray SHG has the potential for even higher surface sensitivity, since second harmonic (SH) photons are generated only from regions with broken centrosymmetry. Note that for hard x-ray radiation (>5 keV; <0.25 nm), the wavelength is small enough that the electric field is sensitive to inhomogeneities on an atomic scale, and the SH is generated throughout the material, rendering it bulk sensitive [24,25]. Instead, soft x-ray SH is generated only from 1–3 atomic layers at surfaces and interfaces of centrosymmetric media, as shown recently in the first demonstration of SXR SHG [16]. SXR SHG provides detailed electronic structure information analogous to that probed by x-ray absorption, with specificity for interfaces and no requirement for smooth surfaces. The elemental specificity of SXR SHG also reduces extraneous signals from interfaces containing other elements in a multilayer system. It is therefore ideally suited for the study of buried interfaces, but experimental proof is thus far lacking.

Here, we demonstrate the application of SXR SHG for probing the buried interface of a boron film with a support layer of Parylene N, a prototypical organic-inorganic interface. In the experiment, we compare the SXR SHG spectra of the boron-vacuum (B-V) and boron–Parylene N (B-PN) interfaces (Fig. 1), providing the first demonstration of probing the element-resolved electronic structure at a buried interface. To compare the interfacial sensitivity of SXR SHG to that of TEY XAS, we measured TEY XAS of similar samples (see Supplemental Materials for details [26] including Refs. [27–41]) using drain current for electron detection. The TEY XAS spectra of the B-V and B-PN samples are largely indistinguishable, because the probe depth of <10 nm is too large. By contrast, the SXR SHG measurements show clear differences between B-V and B-PN interfaces, allowing a detailed determination of the bond characteristics. Accompanying detailed first principles calculations of SXR SHG spectra for both interfaces permits a detailed interpretation, showing that the observed experimental shift between the two spectra is

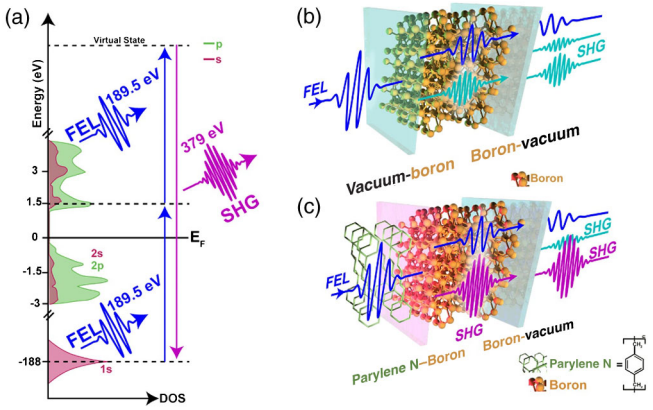

FIG. 1. Schematic of SHG from interfaces. In the energy level diagram (a), the density of states of boron (s-type red, p-type green) is resonantly pumped with an FEL pulse (blue). Because of selection rules, only the p-type states are probed. Two photons at this energy combine in the material and a second harmonic photon at twice the energy (purple) is emitted. The input energy is shown at 189.5 eV, generating a photon of 379 eV. During the experiment, the FEL energy was scanned from 184–196 eV. Two different interfaces were studied here, the (b) boron-vacuum interface and a (c) Parylene N–boron interface. The back boron-vacuum interface also generates some SHG signal (shown in light blue), but it will be less intense due to attenuation of the FEL pulse from transmission through the sample.

due to boron interactions with Parylene N. This indicates a strong surface spectral sensitivity to weak interactions, like London dispersion forces.

At the EIS-TIMEX beamline at the free-electron laser (FEL) FERMI [43], the SHG signal from the sample was detected using the same apparatus as in our recently reported study [16]. Nine different soft x-ray photon energies in the range from 184 to 200 eV were used. These fundamental input energies were just below, at, and just above the boron K edge [44]. The input intensity (I_0) of the FEL was determined from the drain current of an ellipsoidal mirror upstream of the sample. The samples comprised an unsupported 200 nm boron film and a 200 nm boron film with a 100 nm Parylene N support layer, purchased from Lebow Corporation. TEY x-ray absorption spectra of the two materials were collected at Beamline 8-2 at SSRL with the Parylene N layer only 10 nm thick to enhance signal and the sample was mounted on silicon [45,46].

In our previous x-ray SHG study, it was found that the SHG signals were very sensitive to the quality of the FEL laser pulse [16]. Therefore, each FEL shot was filtered by the energy spectrum of the pulse collected before the sample [47]. The intensity of the generated SHG response is given by the relation

$$I_{\mathrm{SHG}} \propto |\chi^{(2)}|^2 I_0^2,$$

where $|\chi^{(2)}|$ is the second order nonlinear susceptibility of the interfacial layer of boron atoms. The SXR SHG

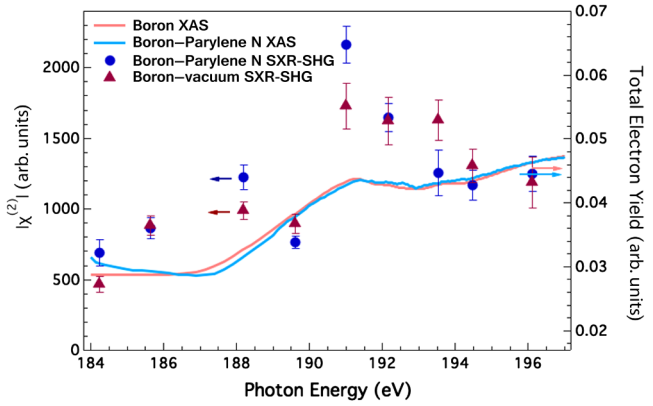

FIG. 2. Second harmonic generation spectra of the boron-vacuum and boron–Parylene N interfaces. The SHG spectrum of the B-V (dark red triangle) and B-PN (dark blue circle) interfaces, shown along with the linear x-ray absorption of the boron film (light red) and boron Parylene N multilayer film (light blue). The arrows indicate the appropriate y axis. The differences in the x-ray absorption spectra are believed to be due to the differences in the background and attempts to correct for it. $|\chi^{(2)}|$, determined from the linear regression slope of the SHG signal vs I_0^2. $|\chi^{(2)}|$, is significantly higher at the boron K edge for B-PN than for B-V. The error in FEL energy is smaller than the width of the marker size.

intensity was plotted proportionally to I_0^2 (assuming constant pulse length and spot size) for each input energy and fit with a linear regression. As can be seen in the equation, the resulting slope is proportional to $|\chi^{(2)}|^2$. Finally, this slope was plotted as a function of photon energy to generate the nonlinear spectrum of the material properties at the surface or interface.

The measured SXR SHG spectra of the B-V and B-PN interfaces are shown in Fig. 2. Resonance effects can be seen in both spectra, as the SXR SHG intensity increases when the fundamental energy is at or above the boron K edge. There is an increase in cross section of B-PN compared to B-V at 188 eV, 191 eV, and a decrease at 193.5 eV. Most notably, we observe a substantial increase in the nonlinear response at energies slightly above the B K-absorption edge. We attribute this to dipole-allowed resonant transitions from 1s to unoccupied states with B p character. The nonlinear response of this spectral region therefore becomes highly sensitive to the electronic valence structure of the interfacial bonds. The second photon absorption process, into a virtual state well above the conduction band to complete the SHG process, is nonresonant and thus less sensitive to the interfacial bonds. Well below and well above the edge, the SXR SHG spectra of B-V and B-PN are within error of each other.

In contrast to SXR SHG results, there are no major differences in the linear TEY spectra of the two materials (Fig. 2). The TEY spectra are essentially identical for both samples, indicating that this technique is insufficiently sensitive to the interface to capture the differences seen in the present SXR SHG spectra. It should be noted that it is possible for some SXR SHG signal to be generated at the back B-V interface, but this contribution will be smaller than that of the front interface due to absorption of the fundamental by the boron layer. More specifically, and as we show, the SXR SHG signal is relevant for analysis at energies above the linear absorption edge, and we operate in direct resonance of the 1s to 2p transition (K edge). The attenuation length for x rays above the edge is approximately 50 nm. Therefore, the FEL beam is largely absorbed in the boron film and the remaining intensity on the rear side is expected to have a small contribution to the SXR SHG signal. In contrast, the generated SXR SHG signal (368 to 392 eV) from the front side is well above the B absorption edge and is therefore only weakly absorbed by the boron slab. Additionally, the back B-V interface is the same for both samples, and so will not affect any qualitative comparisons between the two interfaces. The Parylene N transmits over 90% in the photon energy ranges used here.

First principles electronic structure calculations via perturbation theory within density functional theory [16,48,49] were employed to simulate the SHG response function. Here, the B-V SHG calculation was performed using two layers of boron icosahedral unit cells. In order to understand the influence of the organic molecule on the electronic structure and resulting SXR SHG spectra at the interface, we use boron-ethane (B-E) as a proxy for B-PN for computational feasibility, since both B-E and B-PN have a similar calculated line shape (Supplemental Material, Fig. S7 [26]). Given resonant conditions, the second harmonic signal in this energy range is expected to arise primarily from the top boron layer [13], such that the difference between one layer and multiple layers of ethane in the simulation is negligible.

Our electronic structure calculations reveal a redshift of the SXR SHG spectrum at the boron K edge for B-E, as compared to B-V [Fig. 3(a)]. This is in general agreement with the experimental spectra for B-PN vs B-V, where we find a redshift of less than 2 eV of the main SXR SHG peak at 191 eV. Although for the larger calculation we were forced to use B-E for computational reasons, the differences were small as compared to B-PN [26]. We explored the effect of the interfacial bond length between boron and the organic layer on the simulated spectra in Fig. 3(b), where we find a monotonic blueshift in the 191 eV peak with increasing ethane separation, such that an increase in the separation distance from 0.9 to 1.9 Å resulted in a 2 eV shift, while a further increase to 2.9 Å lead to a further 1 eV shift. This shift is assigned to London dispersion forces as no other strong interactions are present. However, the exact spectral calculations are not quantitative because broadening, inaccuracies of the atomic positions, fluctuations in the molecular motions due to thermal energy, and the calculated spectral ringing are not

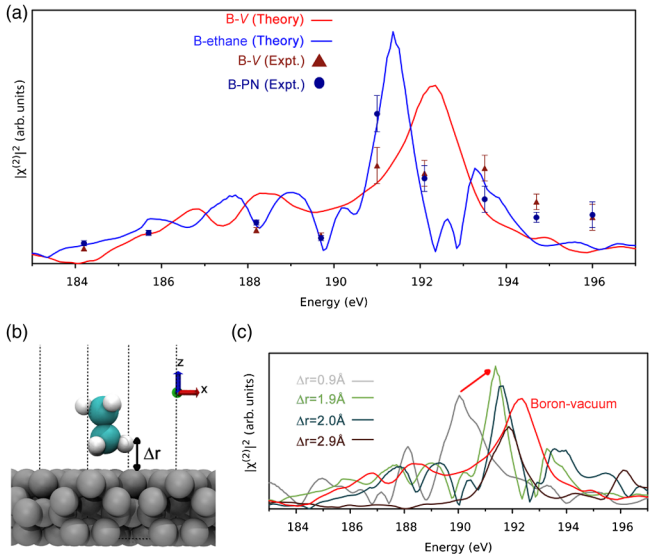

FIG. 3. (a) Comparison of theoretical calculations of SXR SHG boron-vacuum (red line) spectra and boron-ethane spectra (blue) at its equilibrium distance 1.9 Å with the experimental SXR SHG measurements of B-*V* (dark red triangles) and B-PN (dark blue circles). The calculation captures the enhancement of and the blueshift in the 191 eV feature in B-PN compared to B-*V*. (b) Schematic of boron-ethane computational unit cell. We vary the Δr distance between the hydrogen atom and the surface of boron. (c) Comparison of theoretical SXR SHG as a function of distance between boron and ethane, ranging from 0.9 Å (light gray), 1.9 Å (green), 2.0 Å (blue), to 2.9 Å (brown). As distance between the boron and ethane is increased, the primary peak at 191 eV blueshifts in energy (indicated by the red arrow).

accurately represented. A separation distance of 1.9 Å agrees with the minimum energy distance based upon a relaxation within DFT, and is a good match to the experimental SHG spectrum. Of note, an increase in the separation distance from 1.9 to 2.0 Å resulted in a 200 meV spectral shift. As 200 meV is easily resolvable at x-ray FELs, the ability to determine distances with a resolution of 0.1 Å using this computation method has been shown previously, particularly in the bulk [16,42]. This predicted high sensitivity of SXR SHG to interfacial bond length indicates a unique and general technique for elucidating interfacial structure, but due to the low spectral density such a high accuracy cannot be obtained here. Our calculations reveal that ethane induces a shift in the Hartree potential near the interface due to electronic screening, the magnitude of which is strongly dependent on the proximity of the ethane layer to the boron surface. Density of states calculations (Fig. S10 [26]) indicate that the boron core energy levels lie at lower energy in B-*E* compared to B-*V* as a result of this screening. Thus, the experimental spectral differences between B-*V* and B-PN can be attributed to electronic screening in the interfacial boron atoms, rather than to specific interactions, e.g., orbital hybridization.

In conclusion, linear XAS spectra of the B-*V* and B-PN samples exhibited no observable difference between the two samples, whereas SXR SHG reveals distinct differences due to its sensitivity to the interface. This is the first time that a buried interface has been resolved with atom-specific sensitivity. More generally, these experiments clearly demonstrate the sensitivity of SXR SHG to subtle changes in the interfacial electronic structure of the buried interface with sensitivity to a single atomic layer. The results show that SXR SHG is highly sensitive to interfacial bond lengths and to subangstrom bond length changes, resulting in measurable spectral shifts in the hundreds of milli-electron volt range. Under the assumption of comparability of an ethane-boron interfacial bond with a Parylene N–boron interfacial bond, it was possible to determine the bond length to be approximately 1.9 Å. However, the fact that ethane had to be used as a proxy for Parylene N in simulations of varying distance highlights the importance of developing numerical methods to enable computation of larger systems with high fidelity. While SXR SHG spectroscopy clearly is a unique and powerful new tool, profound understanding of interfacial electrodynamics will require a carefully orchestrated duet of theory and experiment. Because of the ultrafast nature of the probe and its sensitivity to single atomic layers, the technique has great potential for future studies of dynamics of buried interfaces in electrochemical cells and catalysts. In the near future, SXR SHG spectroscopy can be used to probe the interfacial electronic structure in a variety of other systems of critical interest, including electronics, batteries, and photocatalytic systems that are difficult to study with other methods. Moreover, the newly revealed high sensitivity to interfacial bond lengths and symmetries will enable unique studies on interfacial strain and its influence on electronic transport properties.

Soft x-ray SHG measurements were conducted at the EIS-TIMEX beamline at FERMI. The research leading to these results has received funding from the European Community's Seventh Framework Programme (FP7/2007-2013) under Grant No. 312284. TEY x-ray absorption spectra were collected at beamline 8-2 at the Stanford Synchrotron Radiation Lightsource, SLAC National Accelerator Laboratory, which is supported by the U.S. DOE, Office of Science, Office of Basic Energy Sciences under Contract No. DE-AC02-76SF00515. C. J. H. and S. L. R. were supported by the U.S. Army Research Laboratory (ARL) and the U.S. Army Research Office (ARO) under Contracts and Grants No. W911NF-13-1-0483 and No. W911NF-17-1-0163. R. K. L. and R. J. S. were supported by the Office of Science, Office of Basic Energy Sciences, Division of Chemical Sciences, Geosciences, and Biosciences of the U.S. Department of Energy at the Lawrence Berkeley National Laboratory (LBNL) under Contract No. DE-AC02-05CH11231. W. S. D. was supported by the Joint Center for Artificial Photosynthesis, a DOE Energy Innovation Hub, supported

through the Office of Science of the U.S. DOE under Award No. DE-SC0004993. S. L. R. received a National Science Foundation Graduate Research Fellowship under Grant No. DGE 1106400. Any opinions, findings, and conclusions or recommendations expressed in this material are those of the author(s) and do not necessarily reflect the views of the National Science Foundation. M. Z. acknowledges support by the Max Planck Society (Max Planck Research Group) and the Federal Ministry of Education and Research (BMBF) under "Make Our Planet Great Again—German Research Initiative" (Grant No. 57427209 "QUESTforENERGY") implemented by DAAD. M. Z. acknowledges funding by the W. M. Keck Foundation, and funding from Laboratory Directed Research and Development Program at Berkeley Lab (107573). P. M. and L. P. were supported by the project Single-Shot X-Ray Emission-Spectroscopy experiments funded by the Italian Ministry for Education and Research as an in-kind project for the EuroFEL consortium. Simulations were performed as part of a user project with S. J., T. A. P., and C. D. P. at The Molecular Foundry (TMF), LBNL. Theoretical simulations of nonlinear susceptibility by C. D. P. were carried out within TIMES at SLAC National Accelerator Laboratory supported by the U.S. Department of Energy, Office of Basic Energy Sciences, Division of Materials Sciences and Engineering, under Contract No. DE-AC02-76SF00515. Portions of the SXR SHG spectra calculations used resources of the National Energy Research Scientific Computing Center, which is supported by the Office of Science of the U.S. Department of Energy under Contract No. DE-AC02-05CH11231. This work also used he Extreme Science and Engineering Discovery Environment (XSEDE), which is supported by National Science Foundation Grant No. ACI-1548562. Material support was provided by the Office of Science, Office of Basic Energy Sciences, Division of Chemical Sciences, Geosciences, and Biosciences of the U.S. Department of Energy at LBNL under the contract listed above. Travel support was provided by ARL and ARO under the contracts and grants listed above. M. Z., R. J. S., and T. A. P. acknowledge funding from the UC Office of the President within the Multicampus Research Programs and Initiatives (M21PL3263).

*cpschwartz@lbl.gov
†wsdrisdell@lbl.gov
‡saykally@berkeley.edu

[1] H. Hong, R. D. Aburano, D.-S. Lin, H. Chen, T.-C. Chiang, P. Zschack, and E. D. Specht, X-Ray Scattering Study of Ag/Si(111) Buried Interface Structures, Phys. Rev. Lett. **68**, 507 (1992).

[2] E. Gann, A. Watson, J. R. Tumbleston, J. Cochran, H. Yan, C. Wang, J. Seok, M. Chabinyc, and H. Ade, Topographic measurement of buried thin-film interfaces using a grazing resonant soft x-ray scattering technique, Phys. Rev. B **90**, 245421 (2014).

[3] N. Shibata, S. D. Findlay, S. Azuma, T. Mizoguchi, T. Yamamoto, and Y. Ikuhara, Atomic-scale imaging of individual dopant atoms in a buried interface, Nat. Mater. **8**, 654 (2009).

[4] P. Han, A. R. Kurland, A. N. Giordano, S. U. Nanayakkara, M. M. Blake, C. M. Pochas, and P. S. Weiss, Heads and tails: Simultaneous exposed and buried interface imaging of monolayers, ACS Nano **3**, 3115 (2009).

[5] J. C. Conboy, J. L. Daschbach, and G. L. Richmond, Total internal reflection second-harmonic generation: Probing the alkane water interface, Appl. Phys. A **59**, 623 (1994).

[6] J. C. Conboy and G. L. Richmond, Examination of the electrochemical interface between two immiscible electrolyte solutions by second harmonic generation, J. Phys. Chem. B **101**, 983 (1997).

[7] A. M. Jubb, D. Verreault, R. Posner, L. J. Criscenti, L. E. Katz, and H. C. Allen, Sulfate adsorption at the buried hematite/solution interface investigated using total internal reflection (TIR)-Raman spectroscopy, J. Colloid Interface Sci. **400**, 140 (2013).

[8] C. T. Williams and D. A. Beattie, Probing buried interfaces with non-linear optical spectroscopy, Surf. Sci. **500**, 545 (2002).

[9] A. J. Hopkins, C. L. McFearin, and G. L. Richmond, Investigations of the solid-aqueous interface with vibrational sum-frequency spectroscopy, Curr. Opin. Solid State Mater. Sci. **9**, 19 (2005).

[10] G. Lüpke, Characterization of semiconductor interfaces by second-harmonic generation, Surf. Sci. Rep. **35**, 75 (1999).

[11] H. Chang, P. E. Ohno, Y. Liu, E. H. Lozier, N. Dalchand, and F. M. Geiger, Direct measurement of charge reversal on lipid bilayers using heterodyne-detected second harmonic generation spectroscopy, J. Phys. Chem. B **124**, 641 (2020).

[12] M. Xiao, T. Lu, T. Lin, J. S. Andre, and Z. Chen, Understanding molecular structures of buried interfaces in halide perovskite photovoltaic devices nondestructively with sub-monolayer sensitivity using sum frequency generation vibrational spectroscopy, Adv. Energy Mater. **10**, 1903053 (2020).

[13] E. Allaria *et al.*, Highly coherent and stable pulses from the FERMI seeded free-electron laser in the extreme ultraviolet, Nat. Photonics **6**, 699 (2012).

[14] E. Allaria *et al.*, Two-stage seeded soft-x-ray free-electron laser, Nat. Photonics **7**, 913 (2013).

[15] N. Rohringer, D. Ryan, R. A. London, M. Purvis, F. Albert, J. Dunn, J. D. Bozek, C. Bostedt, A. Graf, R. Hill, S. P. Hau-Riege, and J. J. Rocca, Atomic inner-shell x-ray laser at 1.46 nanometres pumped by an x-ray free-electron laser, Nature (London) **481**, 488 (2012).

[16] R. K. Lam *et al.*, Soft X-Ray Second Harmonic Generation as an Interfacial Probe, Phys. Rev. Lett. **120**, 023901 (2018).

[17] Sh. Yamamoto *et al.*, Element Selectivity in Second-Harmonic Generation of $GaFeO_3$ by a Soft-X-Ray Free-Electron Laser, Phys. Rev. Lett. **120**, 223902 (2018).

[18] A. J. Achkar, T. Z. Regier, H. Wadati, Y.-J. Kim, H. Zhang, and D. G. Hawthorn, Bulk sensitive x-ray absorption spectroscopy free of self-absorption effects, Phys. Rev. B **83**, 081106(R) (2011).

[19] N. Ottosson, M. Faubel, S. E. Bradforth, P. Jungwirth, and B. Winter, Photoelectron spectroscopy of liquid water and aqueous solution: Electron effective attenuation lengths and emission-angle anisotropy, J. Electron Spectrosc. Relat. Phenom. **177**, 60 (2010).

[20] M. P. Seah and W. A. Dench, Quantitative electron spectroscopy of surfaces: A standard data base for electron inelastic mean free paths in solids, Surf. Interface Anal. **1**, 2 (1979).

[21] S. Hüfner, *Photoelectron Spectroscopy: Principles and Applications* (Springer, Berlin, New York, 1996).

[22] B. H. Frazer, B. Gilbert, B. R. Sonderegger, and G. De Stasio, The probing depth of total electron yield in the sub-KeV range: TEY-XAS and X-PEEM, Surf. Sci. **537**, 161 (2003).

[23] M. Abbate, J. B. Goedkoop, F. M. F. de Groot, M. Grioni, J. C. Fuggle, S. Hofmann, H. Petersen, and M. Sacchi, Probing depth of soft x-ray absorption spectroscopy measured in total-electron-yield mode, Surf. Interface Anal. **18**, 65 (1992).

[24] T. E. Glover, D. M. Fritz, M. Cammarata, T. K. Allison, S. Coh, J. M. Feldkamp, H. Lemke, D. Zhu, Y. Feng, R. N. Coffee, M. Fuchs, S. Ghimire, J. Chen, S. Shwartz, D. A. Reis, S. E. Harris, and J. B. Hastings, X-ray and optical wave mixing, Nature (London) **488**, 603 (2012).

[25] S. Shwartz, M. Fuchs, J. B. Hastings, Y. Inubushi, T. Ishikawa, T. Katayama, D. A. Reis, T. Sato, K. Tono, M. Yabashi, S. Yudovich, and S. E. Harris, X-Ray Second Harmonic Generation, Phys. Rev. Lett. **112**, 163901 (2014).

[26] See Supplemental Material at http://link.aps.org/supplemental/10.1103/PhysRevLett.127.096801 for materials and methods, detailed experimental and theoretical work including analysis of the difference between ethane and parylene N, which includes Refs. [27–42].

[27] L. Poletto, F. Frassetto, P. Miotti, A. Di Cicco, P. Finetti, C. Grazioli, F. Iesari, A. Kivimäki, S. Stagira, and M. Coreno, Spectrometer for X-ray emission experiments at FERMI free-electron-laser, Rev. Sci. Instrum. **85**, 103112 (2014).

[28] G.-R. Yang, Y.-P. Zhao, J. M. Neirynck, S. P. Murarka, and R. J. Gutmann, Chemical-mechanical polishing of polymer films: Comparison of benzocyclobutene (BCB) and parylene-n films by XPS and AFM, MRS Online Proc. Libr. **476**, 161 (1997).

[29] M. A. Barstow, M. Lewis, and R. Petre, Linear absorption coefficient of beryllium in the 50–300-Å wavelength range, J. Opt. Soc. Am. **73**, 1220 (1983).

[30] S. V. Gasilov, A. Ya. Faenov, T. A. Pikuz, I. Yu. Skobelev, F. Calegari, C. Vozzi, M. Nisoli, G. Sansone, G. Valentini, S. de Silvestri, and S. Stagira, Phase-contrast imaging of nanostructures by soft x rays from a femtosecond-laser plasma, Sov. J. Exp. Theor. Phys. Lett. **87**, 238 (2008).

[31] W. F. Beach, A model for the vapor deposition polymerization of *p*-xylylene, Macromolecules **11**, 72 (1978).

[32] S. Ganguli, H. Agrawal, B. Wang, J. F. McDonald, T.-M. Lu, G.-R. Yang, and W. N. Gill, Improved growth and thermal stability of parylene films, J. Vac. Sci. Technol. A **15**, 3138 (1997).

[33] W. Kohn and L. J. Sham, Self-consistent equations including exchange and correlation effects, Phys. Rev. **140**, A1133 (1965).

[34] P. Hohenberg and W. Kohn, Inhomogeneous electron gas, Phys. Rev. **136**, B864 (1964).

[35] A. K. Rappe, C. J. Casewit, K. S. Colwell, W. A. Goddard, and W. M. Skiff, UFF, a full periodic table force field for molecular mechanics and molecular dynamics simulations, J. Am. Chem. Soc. **114**, 10024 (1992).

[36] J. Hutter, M. Iannuzzi, F. Schiffmann, and J. VandeVondele, CP2K: Atomistic simulations of condensed matter systems, WIREs Comput. Mol. Sci. **4**, 15 (2014).

[37] J. P. Perdew and A. Zunger, Self-interaction correction to density-functional approximations for many-electron systems, Phys. Rev. B **23**, 5048 (1981).

[38] P. Prieto, C. Quirós, E. Elizalde, and J. M. Sanz, Electron inelastic mean free path and dielectric properties of a-boron, a-carbon, and their nitrides as determined by quantitative analysis of reflection electron energy loss spectroscopy, J. Vac. Sci. Technol. A **24**, 396 (2006).

[39] N. Bloembergen, R. K. Chang, S. S. Jha, and C. H. Lee, Optical second-harmonic generation in reflection TPDEL-from media with inversion symmetry, Phys. Rev. **174**, 813 (1968).

[40] C. B. Uzundal *et al.*, Polarization-resolved extreme ultraviolet second harmonic generation from $LiNbO_3$, arXiv:2104.01313.

[41] L. Bengtsson, Dipole correction for surface supercell calculations, Phys. Rev. B **59**, 12301 (1999).

[42] E. Berger *et al.*, Extreme ultraviolet second harmonic generation spectroscopy in a polar metal, Nano Lett. **21**, 6095 (2021).

[43] C. Masciovecchio *et al.*, EIS: The Scattering Beamline at FERMI, J. Synchrotron Radiat. **22**, 553 (2015).

[44] A. Majhi, M. Nayak, P. C. Pradhan, E. O. Filatova, A. Sokolov, and F. Schäfers, Soft x-ray reflection spectroscopy for nano-scaled layered structure materials, Sci. Rep. **8**, 15724 (2018).

[45] L. J. Terminello, G. D. Waddill, and J. G. Tobin, High resolution photoabsorption and circular polarization measurements on the University of California/National Laboratory spherical grating monochromator beamline, Nucl. Instrum. Methods Phys. Res., Sect. A **319**, 271 (1992).

[46] K. G. Tirsell and V. P. Karpenko, A general purpose sub-KeV X-ray facility at the Stanford Synchrotron Radiation Laboratory, Nucl. Instrum. Methods Phys. Res., Sect. A **291**, 511 (1990).

[47] M. Zangrando, D. Cocco, C. Fava, S. Gerusina, R. Gobessi, N. Mahne, E. Mazzucco, L. Raimondi, L. Rumiz, and C. Svetina, Recent results of PADReS, the photon analysis delivery and reduction system, from the FERMI FEL commissioning and user operations, J. Synchrotron Radiat. **22**, 565 (2015).

[48] S. Sharma and C. Ambrosch-Draxl, Second-harmonic optical response from first principles, Phys. Scr. **T109**, 128 (2004).

[49] A. Gulans, S. Kontur, C. Meisenbichler, D. Nabok, P. Pavone, S. Rigamonti, S. Sagmeister, U. Werner, and C. Draxl, Exciting: A full-potential all-electron package implementing density-functional theory and many-body perturbation theory, J. Phys. Condens. Matter **26**, 363202 (2014).